Sensitivity of 21st century ocean carbon export flux projections to the choice of export depth horizon

Hilary I. Palevsky[1]* and Scott C. Doney[2]

1. Department of Earth and Environmental Sciences, Boston College, Chestnut Hill, MA, USA
2. Department of Environmental Sciences, University of Virginia, Charlottesville, VA, USA

*Corresponding author: H. I. Palevsky (palevsky@bc.edu)

Key points:

- Projected changes to biological carbon export are evaluated for the first time using the maximum annual (winter) mixed layer depth horizon
- Spatial patterns of projected changes in flux below the winter mixed layer depth differ from those assessed using the 100 m depth horizon
- Differing patterns of projected change are largely driven by strengthened stratification in high latitude regions with deep winter mixing

Abstract

Global Earth system model simulations of ocean carbon export flux are commonly interpreted only at a fixed depth horizon of 100-m, despite the fact that the maximum annual mixed layer depth (MLD_{max}) is a more appropriate depth horizon to evaluate export-driven carbon sequestration. We compare particulate organic carbon (POC) flux and export efficiency (e-ratio) evaluated at both the MLD_{max} and 100-m depth horizons, simulated for the 21st century (2005-2100) under the RCP8.5 climate change scenario with the Biogeochemical Elemental Cycle model embedded in the Community Earth System Model (CESM1-BEC). These two depth horizon choices produce differing baseline global rates and spatial patterns of POC flux and e-ratio, with the greatest discrepancies found in regions with deep winter mixing. Over the 21st century, enhanced stratification reduces the depth of MLD_{max}, with the most pronounced reductions in regions that currently experience the deepest winter mixing. Simulated global mean decreases in POC flux and in e-ratio over the 21st century are similar for both depth horizons (8-9% for POC flux and 4-6% for e-ratio), yet the spatial patterns of change are quite different. The model simulates less pronounced decreases and even increases in POC flux and e-ratio in deep winter mixing regions when evaluated at MLD_{max}, since enhanced stratification over the 21st century shoals the depth of this horizon. The differing spatial patterns of change across these two depth horizons demonstrate the importance of including multiple export depth horizons in observational and modeling efforts to monitor and predict potential future changes to export.

Plain Language Summary

The ocean's biological pump plays an important role in the global carbon cycle by transferring carbon from the surface to the deep ocean, where it can be stored away from contact with the atmosphere. A question that has therefore garnered significant interest is how the biological pump will change over the 21st century under climate change scenarios. Past analyses of global climate model simulations, however, have focused on the amount of carbon that sinks out of the surface-most 100 meters rather than considering the depth that sinking carbon particles must reach in order to be stored away from contact with the atmosphere long term. Here we re-analyze one of these model simulations, introducing the new consideration that, in order to be considered as stored long term, organic carbon particles must sink deep enough to escape the deepest layer mixed into contact with the atmosphere each winter. Using this new definition, we find different spatial patterns for where we expect the biological pump to weaken or strengthen under 21st century climate change. These differences are largely driven by decreases in the depth of deep winter mixing, reducing how deep sinking particles must penetrate in order to be stored long term.

1. Introduction

The ocean plays a critical role in the global carbon cycle, and there is therefore significant interest in projecting how the ocean carbon cycle will respond to and feedback on the trajectory of global climate change over the 21st century. One key component of ocean carbon cycling is the biological pump, in which a fraction of the organic carbon produced by photosynthesis in the surface ocean sinks or is transported into the deep ocean and can be sequestered away from contact with the atmosphere on time scales from months to centuries (Giering & Humphreys, 2018; Le Moigne, 2019; Volk & Hoffert, 1985). Even a small fractional change in the rate of carbon export by the biological pump could have a significant feedback effect on the overall strength of the ocean carbon sink and global carbon cycle, since the overall magnitude of annual export flux (estimated at 5-13 Pg C yr^{-1}; Laws et al., 2011; Siegel et al., 2016) is significantly larger than the current rate at which the ocean absorbs carbon dioxide from the atmosphere (2.6 ± 0.6 Pg C yr^{-1}; Friedlingstein et al., 2019) and is comparable to the current annual rate of fossil fuel carbon emissions (10.0 ± 0.5 Pg C yr^{-1}; Friedlingstein et al., 2019). In addition to influencing the rate at which the ocean absorbs carbon dioxide from the atmosphere, changes to the rate of organic carbon export via the biological pump could influence the future trajectory of ocean acidification and deoxygenation by changing the supply of organic carbon available for respiration in the deep ocean (e.g. Oschlies et al., 2008).

Global Earth system model simulations have consistently agreed that the strength of the biological pump, evaluated as particulate organic carbon (POC) flux through a fixed depth horizon, will decrease over the 21st century under high emissions scenarios of future climate change (Bopp et al., 2001, 2013; Cabré et al., 2015; Fu et al., 2016; Fung et al., 2005; Laufkötter et al., 2016; Schmittner et al., 2008; Steinacher et al., 2010; Taucher & Oschlies, 2011). In order to interpret these simulated changes, analyses generally separate the drivers of POC flux change into two components: changes in the rate of net primary production (NPP), and changes in the fraction of NPP that contributes to POC flux through the fixed 100 m depth horizon (export efficiency, or e-ratio). This builds on efforts to understand and predict the drivers of export efficiency based on empirical algorithms and theoretical models informed by observations of a range of ecosystem factors affecting particle formation, sinking, and remineralization rates (Dunne et al., 2005; Henson et al., 2011; Laws et al., 2000, 2011; Siegel et al., 2014). We focus here on gravitationally-settling POC flux because this component of the overall biological carbon pump has been most widely parameterized, assessed, and validated in Earth system model analyses, but recognize that physical mixing and active transport of both particulate and dissolved organic matter are also critical components of the overall biological pump that warrant further consideration in evaluating how the biological pump will respond to future climate change (Boyd et al., 2019; Le Moigne, 2019).

A number of analyses over multiple generations of model development have identified a pattern in which warming driven by climate change leads to strengthened surface ocean stratification and a concomitant decrease in mixed layer depth, decreasing nitrate supply and increasing light availability for phytoplankton in the surface ocean (Bopp et al., 2001; Fu et al., 2016; Steinacher et al., 2010). This

stratification-driven mechanism has been linked to a global decrease in NPP and POC flux, although the NPP change varies regionally, with production decreasing most strongly in nitrate-limited low latitudes and equatorial regions and in some cases increasing in high latitude regions that had previously been light and iron limited, such as the Southern Ocean (Cabré et al., 2015; Leung et al., 2015). There are also variations among models in the relative influences of stratification-driven decreases in nutrient supply, warming-driven increases in phytoplankton growth rates, and warming-driven increases in grazing that suppress phytoplankton biomass, leading some individual models to project no change or even an increase in global NPP under a 21st century high emissions (RCP8.5) scenario (Laufkötter et al., 2015). In models with multiple phytoplankton functional types, increases in stratification have also been linked to a shift from diatoms towards smaller-celled phytoplankton, which are associated with slower sinking rates and faster remineralization due to reduced mineral ballasting and higher grazing rates, decreasing the e-ratio and thereby further decreasing POC flux (Bopp et al., 2005; Cabré et al., 2015; Marinov et al., 2013). However, detailed analysis of the mechanisms driving e-ratio changes within a subset of models run for the 21st century with RCP8.5 forcing shows discrepancies in their projections of changes to particle formation, sinking, and remineralization rates that together influence the fraction of NPP that contributes to POC flux below the 100 m depth horizon (Laufkötter et al., 2016).

In addition to these ecosystem effects on export flux that have received significant attention, another critical factor in evaluating the impact of changes to the biological pump on the ocean carbon sink under future climate change is how changes in ocean physics will influence the fraction of biologically-produced organic carbon that is sequestered from contact with the atmosphere on climate-relevant timescales. Observational studies have shown that, particularly in high-latitude ocean regions that experience a strong seasonal cycle in mixed layer depth (MLD) with deep winter mixing, a significant fraction of the organic carbon exported from the surface ocean during spring and summer can be remineralized in the seasonal thermocline and ventilated back to the atmosphere during winter, reducing the amount of carbon effectively sequestered (Körtzinger et al., 2008; Palevsky, Quay, Lockwood, et al., 2016; Quay et al., 2012). On a global scale using the spatially-varying maximum annual MLD (MLD_{max}) as the depth horizon that POC must sink below in order to be counted as exported, rather than the fixed 100 m depth horizon generally used in analyzing export in Earth system model output, yields reduced global rates and spatial variability of both POC flux and e-ratio (Palevsky & Doney, 2018). For questions of how the biological pump influences the ocean carbon cycle, the MLD_{max} is a more appropriate choice of export depth horizon than 100 m or other commonly-used choices such as the base of the seasonal mixed layer or the euphotic zone, because it provides a metric for determining the magnitude of carbon sequestration over multiannual time scales.

Based on the increase in stratification as a result of surface warming that has previously been well-documented in 21st century model projections under climate change scenarios, we would also expect the MLD_{max} to shoal over the 21st century as strengthened stratification resists the buoyancy and wind forcing that drives winter mixing. In practice, a shallower MLD_{max} would mean that sinking organic

carbon particles would not have to sink as deep in the water column in order to escape winter mixing. This would be expected to increase the total POC flux below MLD_{max} and the apparent efficiency of that export (i.e. fraction of NPP that leads to export below MLD_{max}), potentially counteracting ecosystem-driven declines in NPP and e-ratio that have previously been identified in model simulations evaluated at the fixed 100 m depth horizon.

In this paper, we test the hypothesis described above by comparing projections of the rate and efficiency of POC flux over the 21st century under a climate change scenario at both MLD_{max} depth horizon and the more commonly-used 100 m depth horizon, using a model and scenario (RCP8.5) that have been widely studied by previous authors. We show significant spatial differences in the projections of export flux and e-ratio over the 21st century when evaluated at the MLD_{max} rather than the 100 m depth horizon, assess the relative influences of ecosystem- and ΔMLD_{max}-based drivers of projected changes in POC flux at the MLD_{max} depth horizon, and discuss implications for both model- and observation-based analyses of the future trajectory of the ocean's biological carbon pump.

2. Methods

2.1 Model description

We analyze model output from the ocean component of a fully coupled, carbon cycle-enabled simulation of the Community Earth System Model (CESM1/CCSM4; Gent et al., 2011; Lindsay et al., 2014) for the 21st century (2005-2100) at nominal 1° resolution with CO_2 emissions and other anthropogenic factors prescribed following the RCP8.5 scenario. The specific simulation analyzed here was chosen because it archived depth-resolved monthly NPP and POC flux for all grid cells throughout the full 21st century simulation. The original output (case name b40.rcp8_5.1deg.001) is publicly available at: http://www.cesm.ucar.edu/experiments/cesm1.0/

The module implementing marine biogeochemical and ecosystem processes within this simulation is the Biogeochemical Ecosystem Model (BEC; Moore et al., 2013), which has been widely used over multiple generations of model development prior to the version used here. BEC has been extensively described and validated elsewhere (Doney et al., 2009; Moore et al., 2004, 2013), but we summarize here key features of the model relevant to biological carbon flux rates and efficiency. BEC includes three explicit phytoplankton functional types (diatoms, small phytoplankton, and diazotrophs), as well as implicit calcification, simulated as a variable fraction of the small phytoplankton group, and a single adaptive zooplankton type. The model includes five nutrients (nitrate, ammonia, phosphate, silicate, and iron), with variable nutrient uptake rates by each phytoplankton group. Particulate organic matter is produced by phytoplankton aggregation, grazing, and zooplankton mortality, but is not represented within BEC as an explicit particle concentration because sinking is implemented implicitly such that particles are immediately remineralized with depth throughout the water column underlying the grid cell in which they were produced (Laufkötter et al., 2016; Moore et al., 2004). The baseline remineralization length scale for POC is 200 meters, but is modified by ballasting effects when associated

with silicate, calcium carbonate, or lithogenic dust, which all increase the remineralization length scale (Moore et al., 2004, 2013).

2.2 Model analysis

We analyze POC flux and e-ratio within this model output evaluated at both the fixed 100 m depth horizon commonly archived and analyzed in model analyses, and at the temporally- and spatially-varying maximum annual MLD (MLD_{max}) depth horizon:

$$\mathrm{POCflux}(z,t) = \mathrm{NPP}(t) \times \text{e-ratio}(z,t) \qquad (1)$$

where z represents the depth horizon (either 100 m or MLD_{max}) and t represents the time period of analysis. We calculate the time-varying MLD_{max} depth horizon in each individual grid cell in each year as the maximum of all monthly MLD values for that grid cell throughout that year. We note that the use of the monthly mean MLD to perform this calculation can yield MLD_{max} values that are shallower than the deepest MLD reached on a single day of deep winter mixing. However, given the time scale of gas exchange (~weeks), particularly in the context of deep MLDs, the use of monthly mean MLD to determine MLD_{max} provides a reasonable approximation of the layer effectively ventilated to the atmosphere each winter. To assess changes in POC flux and e-ratio over time at both depth horizons, we calculate climatological mean values over 20-year periods at both the beginning (t = 2005-2024) and end (t = 2081-2100) of the simulation. All calculations are performed on the native model grid before final results are regridded for plotting.

Observational data available to validate POC flux simulated in the model are limited, such that prior validation of BEC POC flux has by necessity relied on relatively small data sets (e.g. Lima et al., 2014) or on satellite-based algorithms (e.g. Laufkötter et al., 2016) that in turn have been developed using the limited number of in situ observations and therefore may not fully represent global patterns of POC flux and e-ratio (Palevsky, Quay, & Nicholson, 2016; Quay et al., 2020). However, the analysis conducted here focuses on comparisons between the 100 m and MLD_{max} depth horizons and change over time, rather than on absolute rates and patterns, reducing the sensitivity of our results to potential issues in the model's baseline rates and patterns of POC flux. Furthermore, comparison of the BEC model used here with other Earth system model simulations of POC flux and e-ratio have shown that BEC is largely representative of the overall patterns observed across the broad suite of CMIP5 models (Cabré et al., 2015; Laufkötter et al., 2016).

3. Results and Discussion

3.1 Influence of choice of depth horizon on rates and spatial patterns of POC flux and e-ratio

We first compare baseline rates of POC flux and e-ratio (POC flux/NPP) from the beginning of the 21st century (2005-2024), evaluated at both the fixed 100 m and MLD_{max} depth horizons (Figure 1).

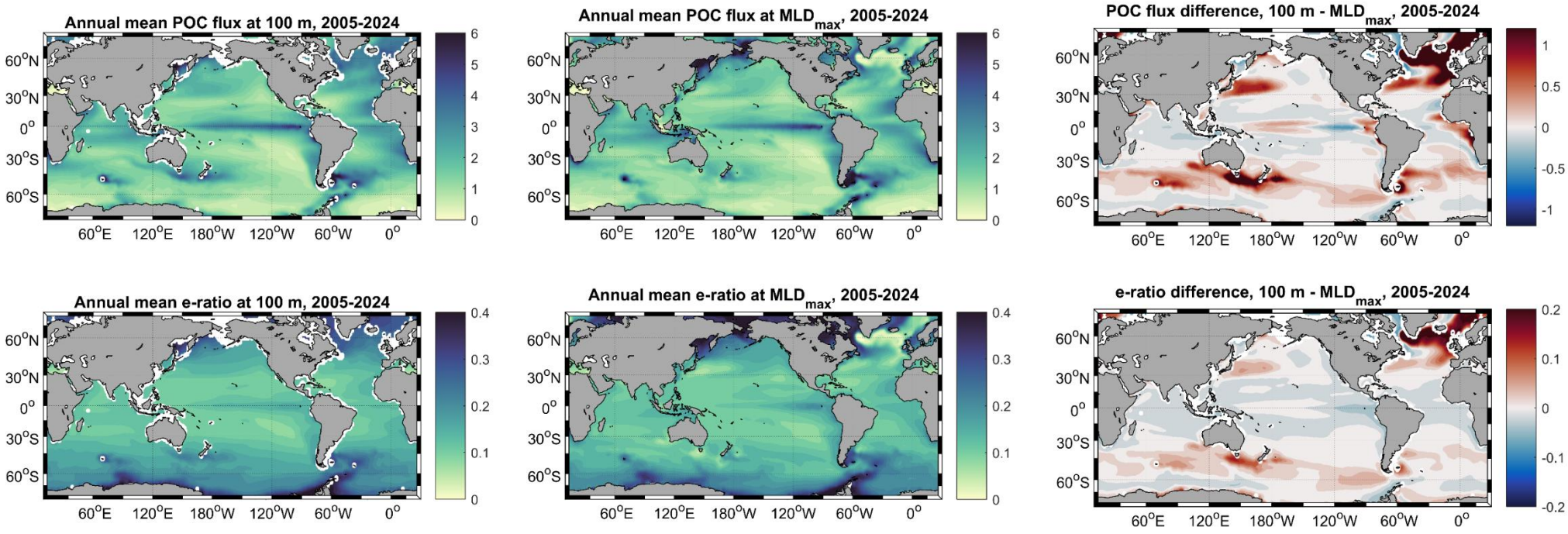

Figure 1. Baseline maps of the spatial patterns of POC flux (top; mol C m^{-2} yr^{-1}) and e-ratio (bottom) evaluated at both the 100 m depth horizon (left) and at the maximum annual mixed layer depth (MLD_{max}) depth horizon (middle) for the beginning of the 21st century (climatological mean from 2005-2024). Spatial patterns of the differences between POC flux and e-ratio evaluated at the two different depth horizons (left panel minus middle panel for each row) are shown in the right-hand plots.

This comparison shows the influence of the choice of depth horizon on both global rates and spatial patterns of export, consistent with results from an earlier, coarser resolution version of this model in a pre-industrial control simulation (Palevsky & Doney, 2018). Spatial patterns in POC flux and e-ratio at the 100 m depth horizon in a similar BEC simulation have previously been described in detail by Laufkötter et al. (2016) and shown to largely match patterns from satellite algorithms of POC flux calibrated with observational data (Dunne et al., 2007; Henson et al., 2012). Briefly, analysis at the 100 m depth horizon shows a band of elevated POC flux and e-ratio driven by equatorial upwelling and generally higher POC flux and e-ratio in subpolar than in subtropical latitudes, largely driven by the model's patterns of NPP (Figure 1a, d). These overall spatial patterns are also evident when evaluated at the spatially-varying MLD_{max} depth horizon (Figure 1b, e), though with significantly lower annual mean POC flux and e-ratio in regions with deep MLD_{max} (Figure 2a), especially in the subpolar North Atlantic, northwest Pacific, and Southern Ocean, when evaluated when evaluated at MLD_{max} (Figure 1c, f). This is due to remineralization of sinking POC between 100 m and MLD_{max} in regions of deep winter mixing, such that a fraction of the carbon that escapes below the 100 m depth horizon is returned to inorganic carbon above MLD_{max} rather than sinking deep enough to be sequestered on annual or longer timescales.

3.2 Change in maximum annual mixed layer depth (MLD_{max}) over the 21st century

We next evaluate simulated changes in MLD_{max} over the 21st century, expected based on prior analyses of model output showing strengthening stratification under climate change scenarios (e.g. Capotondi et al., 2012; Fu et al., 2016). The climatological MLD_{max} at the beginning of the 21st century (2005-2024) shows patterns consistent with observations (Figure S1), with especially deep winter mixing in the subpolar North Atlantic, as well as areas of deep mixing in the western subarctic North Pacific and Southern Ocean (Figures 2a, S1). Although these spatial patterns remain in MLD_{max} simulated at the end of the century (2081-2100; Figure 2b), comparison between MLD_{max} at the beginning and end of the century (Figure 2c) shows a near uniform global shoaling of MLD_{max}, with the few regions where the model simulates an increase in winter mixing reflecting spatial displacement of deep mixing regions in response to changing circulation patterns. The decreases in MLD_{max} over the 21st century are especially pronounced in regions that feature the deepest winter mixing at the beginning of the simulation period, evident in both proportional and absolute changes in MLD_{max} (Figures 2 and S2-3).

This is consistent with prior analyses across multiple generations of model comparison projects showing broad global increases in stratification, with the largest stratification increases found in the regions with the deepest climatological mixed layers at the beginning of the analysis period (Capotondi et al., 2012; Fu et al., 2016). These changes in stratification are driven primarily by enhanced surface warming, although surface freshening plays a significant role in the high latitudes, particularly in the subpolar North Atlantic, where reductions in deep winter convection and the strength of the Atlantic Meridional Overturning Circulation driven by surface ocean warming and freshening have previously been described in analyses of CMIP5 simulations under RCP8.5 (Cheng et al., 2013; Fu et al., 2016).

Detailed assessment of Southern Ocean winter mixed layer formation in CMIP5 models has shown a shallow bias in simulations of winter convection, indicating that models may underestimate future shoaling of winter mixed layer depths, though CESM was among the better-performing models analyzed, avoiding some of the most common systematic biases in stratification strength and location of deep mixing regions (Sallée et al., 2013).

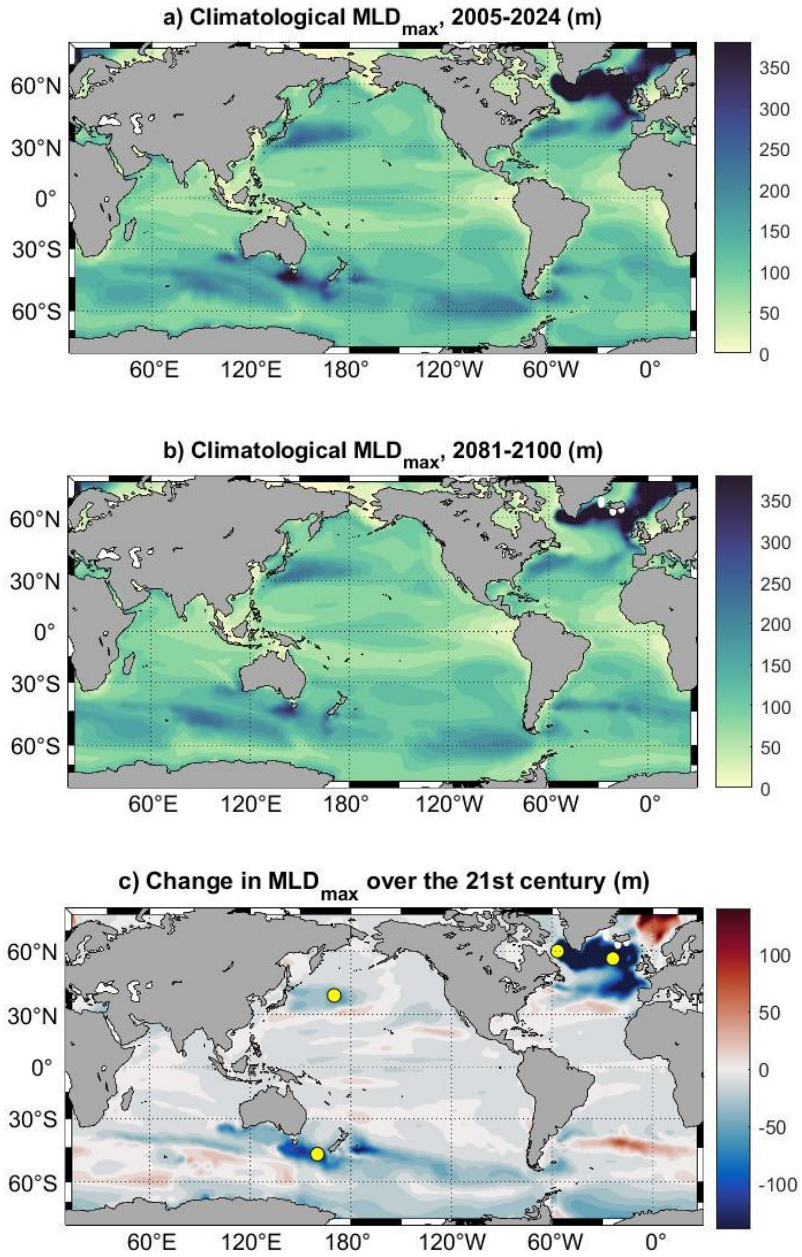

Figure 2. a-b) Maximum annual mixed layer depth (MLD_{max}) for a) the beginning of the 21st century, 2005-2024 and b) the end of the 21st century, 2081-2100, as well as c) the change in MLD_{max} from 2005-2024 to 2081-2100, all from CESM1-BEC following the RCP 8.5 emissions scenario. Yellow circles in (c) are locations where the time evolution over the 21st century is shown in Figure 5.

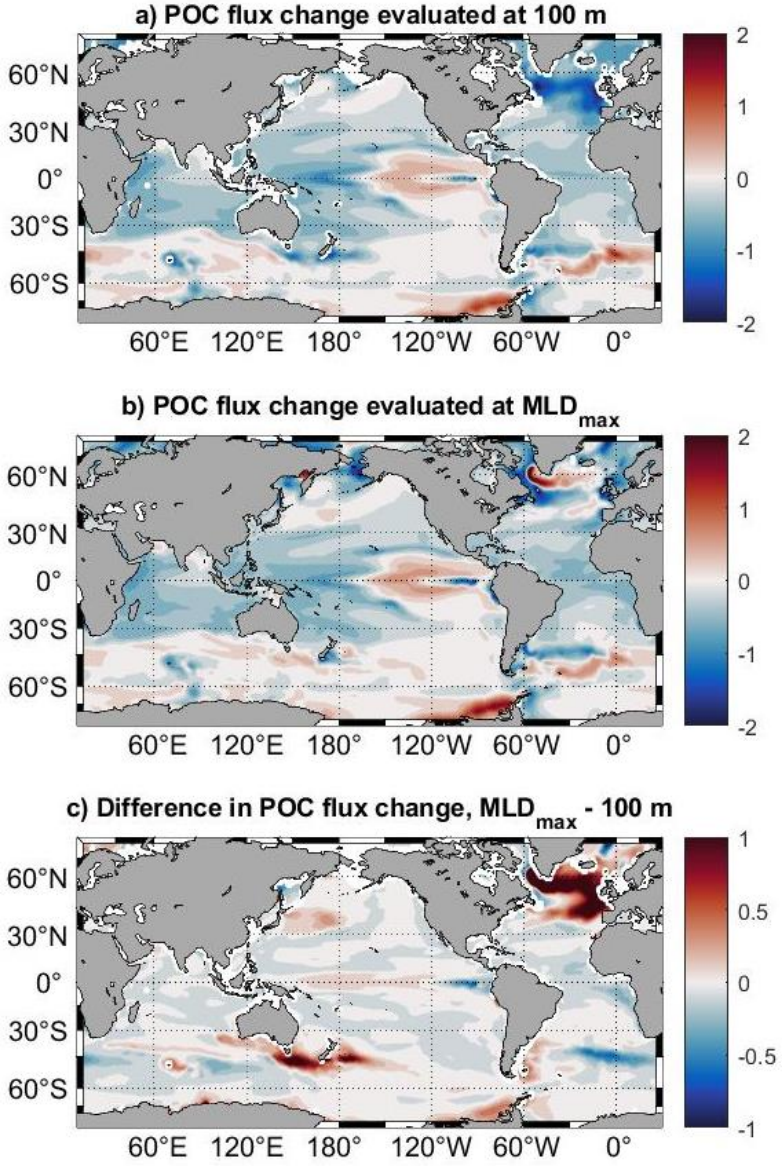

Figure 3. Change in POC flux (mol C m^{-2} yr^{-1}) over the 21st century (2081-2100 minus 2024-2005) under the RCP8.5 scenario in CESM1-BEC, evaluated as flux through a) the fixed 100 m depth horizon, and b) the time-varying MLD_{max} depth horizon. c) Difference between the changes in POC flux over the 21st century determined when using the MLD_{max} versus the 100 m depth horizons (difference between Figures 3b and 3a).

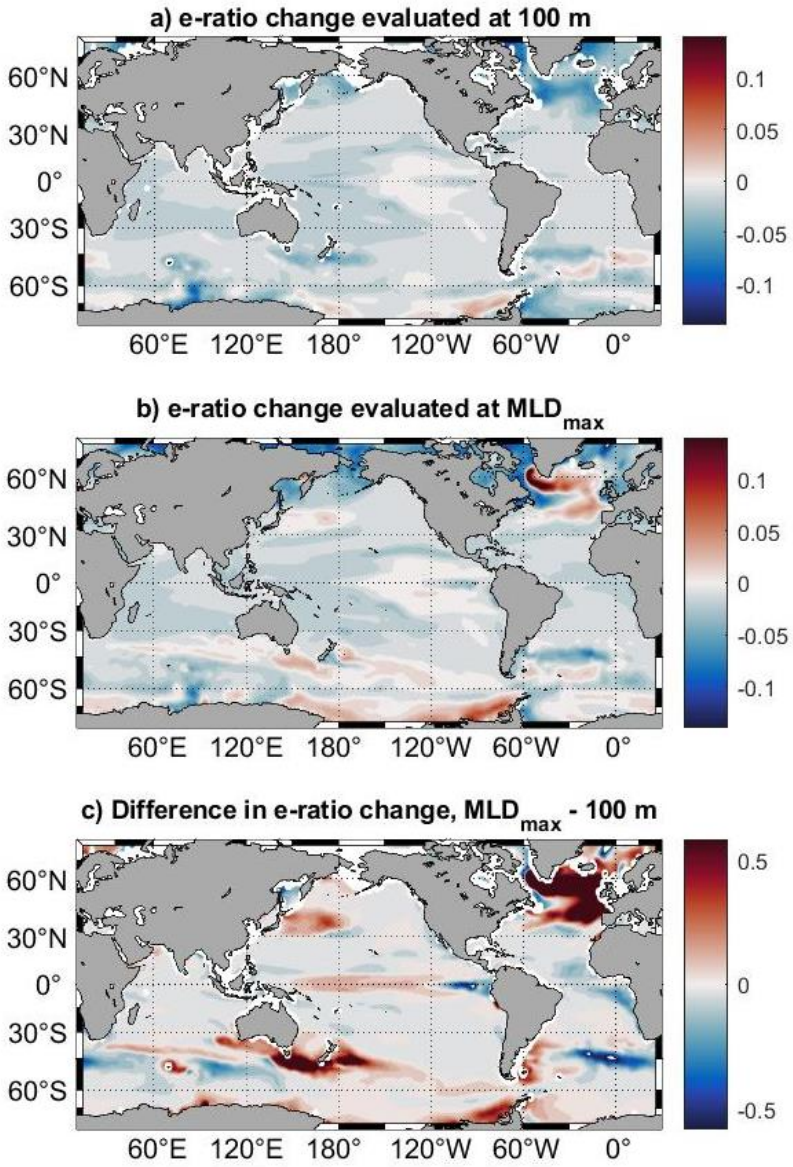

Figure 4. Change in e-ratio (POC flux/NPP) over the 21st century (2081-2100 minus 2024-2005) under the RCP 8.5 scenario in CESM1-BEC, evaluated as flux through a) the fixed 100 m depth horizon and b) the time-varying MLD_{max} depth horizon. c) Difference between the changes in e-ratio over the 21st century determined when using the MLD_{max} versus the 100 m depth horizons (difference between Figures 4b and 4a).

3.3 Change in export flux and efficiency over the 21st century

We evaluate the change in climatological mean export flux (Figure 3) and efficiency (e-ratio; Figure 4) between the beginning and end of the 21st century, evaluated at both the 100 m and MLD_{max} depth horizons. Consistent with prior analyses focused on change at the 100 m depth horizon (Bopp et al., 2013; Cabré et al., 2015; Fu et al., 2016; Laufkötter et al., 2016), the overall global rate and efficiency of export flux through the 100 m depth horizon is projected to decrease over the 21st century (Figures 3a and

4a). The exceptions to this overall global pattern are in the eastern tropical Pacific and the Southern Ocean, which show projected increases in POC flux through the 100 m depth horizon over the 21st century, though it is important to note in interpreting these patterns that these are regions where comparison across multiple models have shown the largest disagreements in the sign and spatial patterns of projected changes (Laufkötter et al., 2016). These regions of projected increases in POC flux at the 100 m depth horizon are predominantly driven by projected increases in NPP in these regions, as the e-ratio at 100 m is projected to decrease nearly everywhere throughout the global ocean, excepting a few regions within the Southern Ocean (Figure 4a).

Integrated globally, the fractional change in POC flux and e-ratio over the 21st century within this simulation is not significantly different when evaluated at MLD_{max} rather than the 100 m depth horizon. Global mean POC flux decreases by 8.6% from 7.9 to 7.2 Pg C/yr at 100 m and by 7.6% from 7.7 to 7.1 Pg C/yr at MLD_{max} and the global mean e-ratio decreases by 5.6% from 0.148 to 0.139 at 100 m and by 4.0% from 0.143 to 0.137 at MLD_{max}. However, spatial differences are pronounced. Projected decreases in export flux and efficiency determined at the 100 m depth horizon are significantly mitigated or even in some cases reversed in sign in regions that experience especially deep winter mixing at the beginning of the century and strong shoaling of MLD_{max} over the course of the century. Conversely, in regions where MLD_{max} is shallower than 100 m, in the tropical and subtropical Atlantic, eastern tropical Pacific, and subtropical Pacific, absolute rates of decrease in POC flux and e-ratio are lesser when evaluated at the shallow MLD_{max} depth horizon rather than at 100 m. These opposing spatial changes are largely balanced, leading to similar fractional global changes when comparing across the MLD_{max} and 100 m depth horizons. However, we note that this result may be model-specific due to the sensitivity of the globally integrated change to even minor MLD biases and differences in simulated regional patterns of export and remineralization length scales that could influence the magnitude of opposing spatial patterns of change between the high latitude deep MLD_{max} regions and low latitude shallow MLD_{max} regions.

We highlight four locations with deep MLD_{max} at the beginning of the 21st century to illustrate the influence of winter mixing on the evolving rates and efficiency of export in these regions (Figure 5). These sites, located in the Labrador Sea, Iceland Basin, Kuroshio Extension region of the western subarctic North Pacific, and in the western South Pacific sector of the Southern Ocean, all experience a decrease in MLD_{max} over the course of the 21st century, though the decreases at the North Pacific and Southern Ocean sites remain within the range of internal variability from the beginning of the century (determined by comparing the mean ± standard deviation of the first and last 10 years of the time series). All sites show the expected pattern of changes in POC flux and e-ratio, where POC flux and e-ratio both increase with depth within the top portion of the euphotic zone where NPP exceeds respiration, reaching a maximum below which remineralization dominates and reduces POC flux and e-ratio with depth. In each of these locations, MLD_{max} is significantly below the compensation depth, in the portion of the water column where both POC flux and e-ratio decrease with depth. These decreases in POC flux and e-ratio

through the water column mean that a shoaling MLD_{max} will increase the rate and efficiency of POC flux through the MLD_{max} depth horizon, independent of any ecosystem driven changes that might affect the rate and efficiency of export. The time evolution at these four sites illustrates that POC flux and e-ratio are simulated to decrease over the 21st century across all fixed depth horizons, consistent with previous analyses focused on the 100 m depth horizon (Bopp et al., 2013; Cabré et al., 2015; Fu et al., 2016; Laufkötter et al., 2016). However, the simultaneous decrease in the MLD_{max} depth horizon that sinking particles must cross in order to be sequestered – evident at all sites, but particularly pronounced at the Labrador Sea and Iceland Basin sites – yields a net increase in POC flux and e-ratio over the 21st century when evaluated at the shoaling MLD_{max} depth horizon.

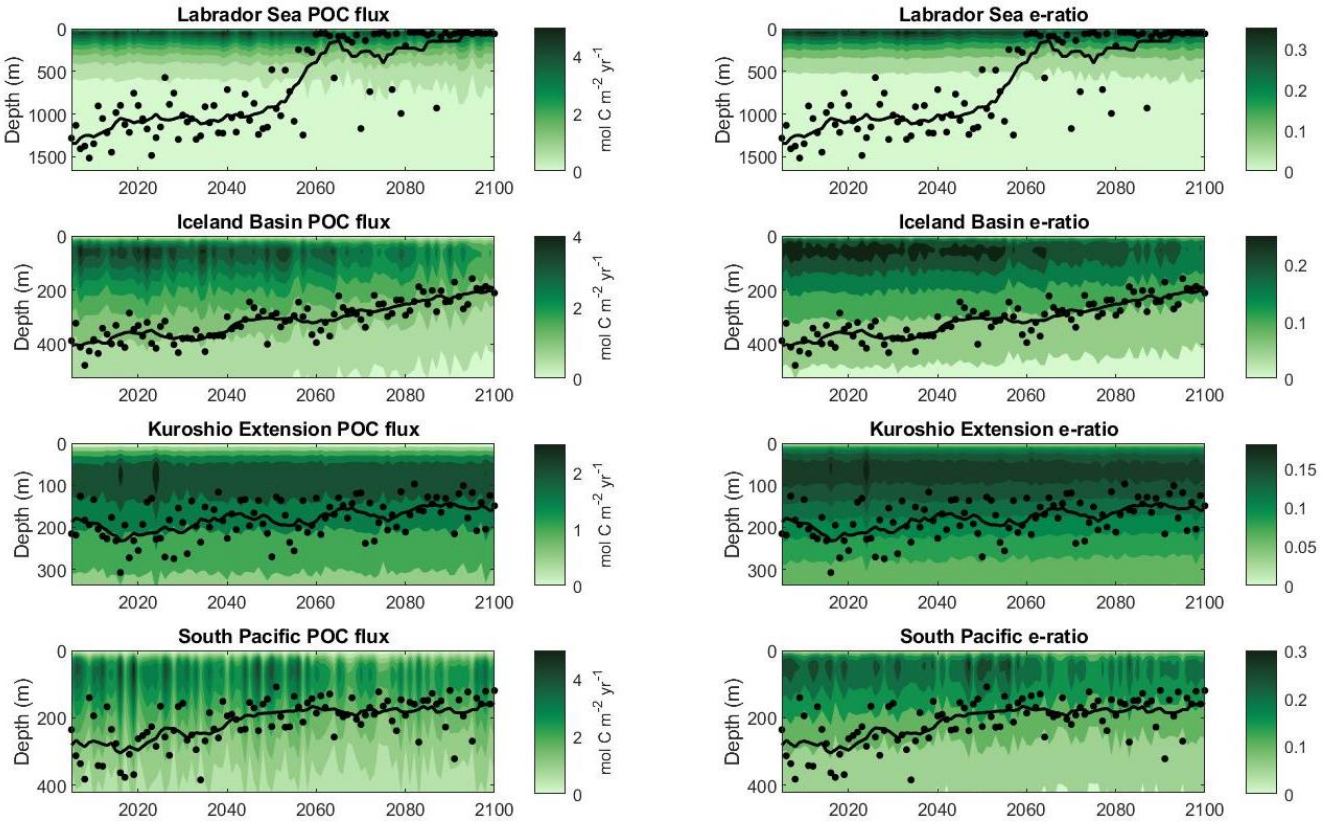

Figure 5. Time evolution of POC flux (left) and e-ratio (right) with depth over the 21st century under RCP8.5 for four example sites at locations with deep winter mixing (locations shown in Figure 2c). MLD_{max} for each year in the simulation is shown in the black dots and the 10-year running mean MLD_{max} is shown in the black lines. Note the differences in depth range and color bars across sites.

3.4 Taylor decomposition of changes to export flux at the MLD_{max} depth horizon

The changes described above in POC flux and e-ratio evaluated at the time-varying MLD_{max} depth horizon are influenced both by changes in ecosystem dynamics and by shoaling of the MLD_{max} depth horizon. Laufkötter et al. (2016) have previously investigated the ecosystem-based drivers of change in POC flux over the 21st century at the fixed 100 m depth horizon by using a Taylor decomposition of equation (1) where z = 100 m to separate the effects of changes in NPP from changes in e-ratio driven by changes in particle production, sinking, and remineralization. In order to separate the influence of the change in MLD_{max} from these ecosystem-dependent effects, we build on their approach by taking a first-order Taylor decomposition of equation (1) where z = $MLD_{max,}$, adding an additional term in the decomposition to account for change in the MLD_{max} depth horizon over time.

$$\frac{\partial \mathrm{POCflux}_{\mathrm{MLDmax}}}{\partial \mathrm{t}} = \left(\frac{\partial \mathrm{NPP}}{\partial \mathrm{t}} \times \text{e-ratio}\right)_{\mathrm{MLDmax,2005-2024}} + \left(\frac{\partial \text{e-ratio}}{\partial \mathrm{t}} \times \mathrm{NPP}\right)_{\mathrm{MLDmax,2005-2024}} + \left(\mathrm{NPP} \times \frac{\partial \text{e-ratio}}{\partial \mathrm{z}}\right) \times \frac{\partial \mathrm{MLDmax}}{\partial \mathrm{t}_{\mathrm{2005-2024\ to\ 2081-2100}}} + \mathrm{Residual} \quad (2)$$

The first and second terms on the right-hand side represent the effects of changes in NPP and in e-ratio on POC flux through the climatological mean MLD_{max} from 2005-2024. By using $MLD_{max,2005\text{-}2024}$ as a spatially variable but temporally fixed depth horizon to evaluate these two terms, we isolate these influences from the effects of change over time in MLD_{max}. The NPP and e-ratio terms are analogous to the same terms from the Taylor decomposition method previously applied by Laufkötter et al. (2016) to interpret ecosystem-based influences on POC flux through the fixed 100 m depth horizon (their equation 18). Following the methodology of Laufkötter et al., the partial derivatives $\frac{\partial}{\partial t}$ are computed by taking the difference between the end of the century (2081-2100) and beginning of the century (2005-2024) averages.

The third term on the right hand side represents the effect on POC flux of changes in MLD_{max} over time. Evaluating this term necessitates selecting a time point at which to evaluate $\left(\mathrm{NPP} \times \frac{\partial \text{e-ratio}}{\partial \mathrm{z}}\right)$, as the ecosystem effects captured in the first two terms also change the shape of the POC flux depth profile over time. Depth profiles at the sites with deep winter mixing profiled in Figure 5 show that $\frac{\partial \mathrm{POCflux}}{\partial \mathrm{z}}$ (shown in Figure S4) and $\frac{\partial \text{e-ratio}}{\partial \mathrm{z}}$ decrease over the course of the 21st century – i.e. the transfer efficiency to depth from below the euphotic zone increases over time. Given this, we make the conservative choice to evaluate the ΔMLD_{max} term in the Taylor decomposition using POC flux (i.e. NPP × e-ratio) from 2081-2100, so that any bias introduced by the selection of the evaluation time point will tend to decrease rather than increase the size of this term. We therefore calculate the ΔMLD_{max} term as the difference between the mean POC flux from 2081-2100 evaluated at the MLD_{max} depth horizon from

2081-2100 versus at the MLD_{max} depth horizon from 2005-2024. The residual term that accounts for non-linear effects is close to zero in most locations, allowing us to quantitatively assess the relative contributions of changes in NPP, e-ratio, and MLD_{max} changes to the simulated change in POC flux through the MLD_{max} depth horizon.

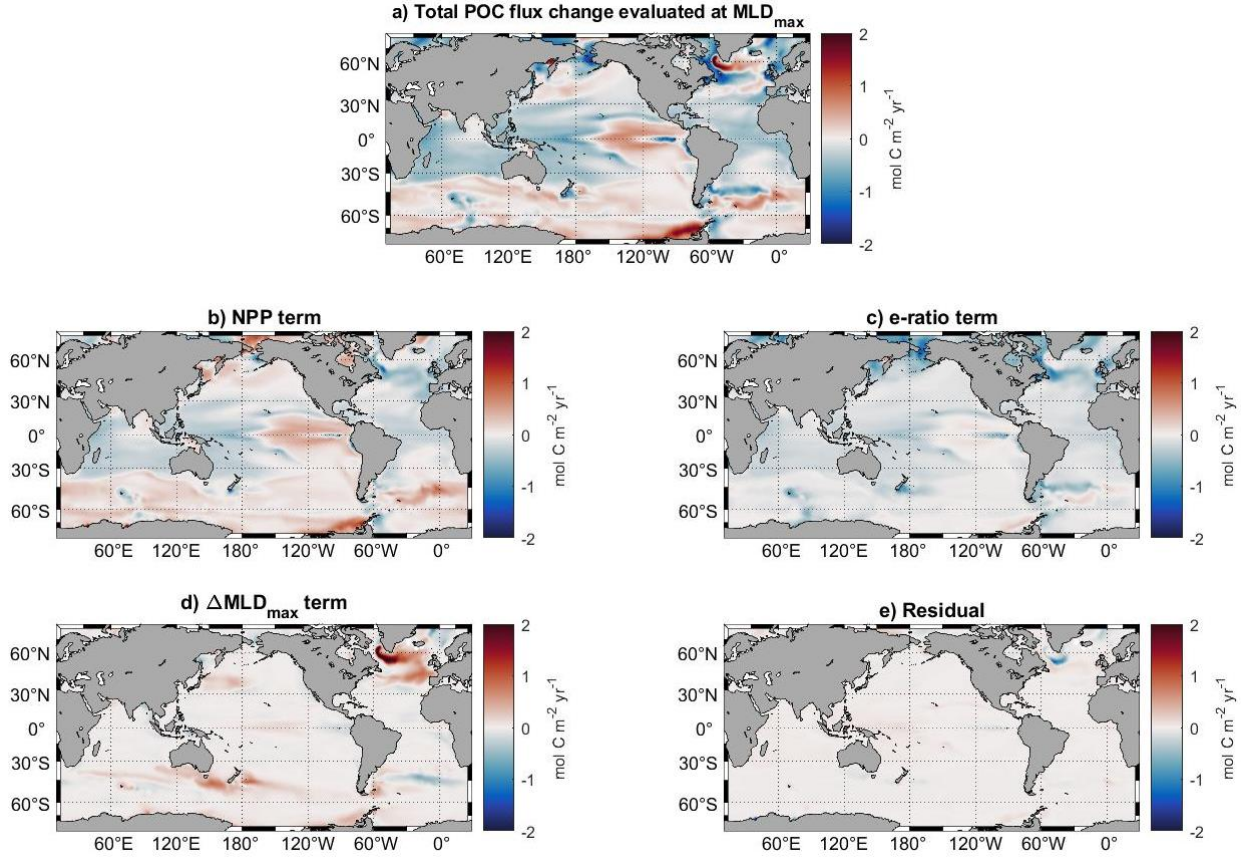

Figure 6. 1st order Taylor decomposition of the change in POC flux over the 21st century, evaluated at the MLD_{max} depth horizon following equation 2. Components of the a) total change in POC flux at MLD_{max} (also shown in Figure 3b) were separated into changes due to b) change in NPP, c) change in e-ratio independent of the change in depth horizon, and d) change due to change in the MLD_{max} depth horizon, plus e) the residual of the decomposition.

Global maps of the Taylor decomposition of the change over the 21st century in POC flux at MLD_{max} are shown in Figure 6. The ecosystem-based influences of change in NPP (Figure 6b) and e-ratio through a fixed depth horizon (Figure 6c) are consistent with previous analysis by Laufkötter et al. (2016) focused on changes through the fixed 100 m depth horizon (explicitly reproduced in Figure S5 with spatial maps analogous to those in Figure 6). NPP is simulated to decrease globally by 4% over the 21st century, although with regional increases in the equatorial Pacific and Southern Ocean that are the primary driver of corresponding patterns of increasing POC flux through the MLD_{max} depth horizon in these regions. Regional patterns of NPP change are driven by a combination of competing effects from stratification-driven reduction in both nutrient supply and light limitation, and warming-driven

stimulation of both phytoplankton growth and grazing pressure (Laufkötter et al., 2015). Large-scale spatial patterns in POC flux change (Figure 6a) largely match those of the NPP term (Figure 6b), particularly in regions with pre-existing strong stratification and restricted MLD_{max} depths today. The e-ratio through the fixed 2005-2024 MLD_{max} depth horizon decreases nearly everywhere globally, similar to the decrease in e-ratio at the fixed 100 m depth horizon (Figure 4a), contributing towards decreasing POC flux over the 21st century (Figure 6c). These changes are likely driven by the decreases in particle formation through phytoplankton aggregation and changes in phytoplankton functional type that influence the ballasting-dependent remineralization length scale previously shown to drive e-ratio change at 100 m (Laufkötter et al., 2016), though the regions with the deepest MLD_{max} from 2005-2024 are also strongly influenced by factors controlling transfer efficiency through the mesopelagic, which can differ from controls on e-ratio in the surface ocean (Lima et al., 2014).

Having now separated out the effects of the ecosystem-based factors, we isolate the influence of physical stratification-driven decreases in MLD_{max} on the change in POC flux through the MLD_{max} depth horizon (Figure 6d). Decreases in MLD_{max} from 2005-2024 to 2081-2100 increase the rate at which particles escape below this shoaling depth horizon, with spatial patterns of stratification-driven increases in export closely matching the spatial patterns of the decrease in MLD_{max} itself (Figure 2c). In regions with deep winter mixing and strong shoaling of MLD_{max} over the 21st century, notably the subpolar North Atlantic, the western subarctic North Pacific and the Pacific sector of the Southern Ocean, the overall POC flux change through the MLD_{max} depth horizon is predominantly driven by this increase in stratification rather than by the ecosystem-dominated NPP and e-ratio changes.

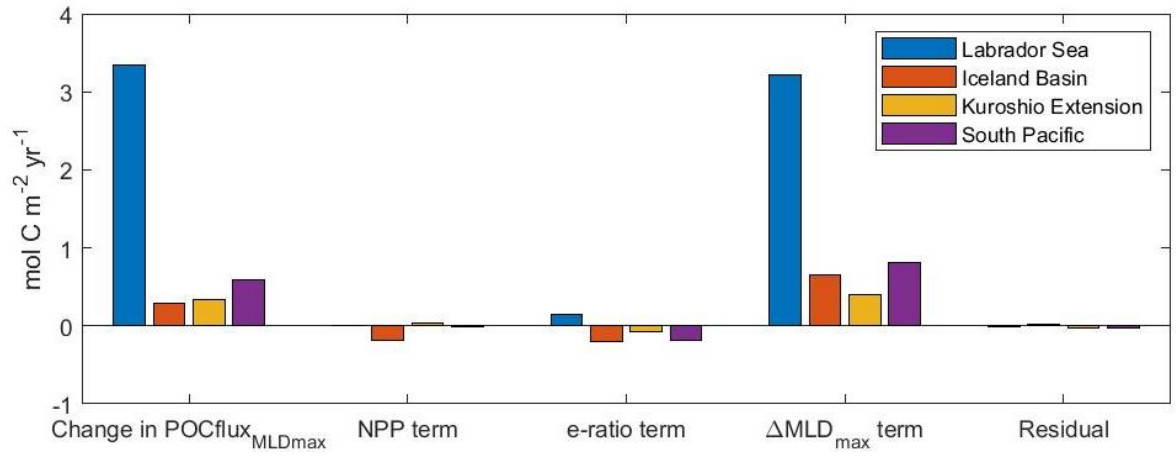

Figure 7. Taylor decomposition of the factors driving the change in POC flux at the MLD_{max} depth horizon over the 21st century at each of the four example sites with deep winter mixing (locations shown in map view in Figure 2c and time evolution with depth at each site shown in Figure 5).

To illustrate this, we highlight the Taylor decomposition at the four sites with deep winter mixing at the beginnng of the 21st century from Figure 5, showing the importance of the change in MLD_{max} on the overall change in POC flux through this depth horizon (Figure 7). At each of these deep winter mixing locations, POC flux increases over the 21st century when evaluated at $MLD_{max.}$ The ecosystem effects on POC flux are mixed across these sites. NPP decreases in the Iceland Basin, increases slightly in the Kuroshio Extension, and changes negligibly in the Labrador Sea and South Pacific, driving proportional changes in POC flux. The e-ratio through the beginning-of-the-century MLD_{max} depth horizon decreases in the Iceland Basin, Kuroshio Extension, and South Pacific sites, consistent with the near-uniform global decrease in e-ratio evaluated at the fixed 100 m depth horizon (Figure 4a). However, at the Labrador Sea site, though the e-ratio decreases over the 21st century at the fixed 100 m depth horizon, it instead increases at the much deeper beginning-of-the-century MLD_{max} depth horizon (1180 ± 220 m). This highlights the importance of considering not only the ecosystem factors that influence the efficiency of export from the surface ocean, but also the transfer efficiency of particles through the mesopelagic. Prior work has shown that e-ratio at the base of the euphotic zone and transfer efficiency from base of the euphotic zone to the deep ocean (1000-2000 m) have opposing spatial distributions, with high transfer efficiency but low e-ratios in the oligotrophic regions in the subtropical gyres and low transfer efficiencies in more productive high latitude regions (Lam et al., 2011; Lima et al., 2014; Marsay et al., 2015). Transfer efficiency from the compensation depth (or 100 m) to 2000 m increases over the 21st century in the Labrador Sea, Iceland Sea, and South Pacific, with negligible change in the Kuroshio Extension (Figure S4), consistent with a shift towards a more oligotrophic-type ecosystem. However, the largest term in the Taylor decomposition at each of these sites is the influence of the shoaling MLD_{max} depth horizon, which is the dominant factor driving the projected decrease in POC flux over the 21st century at the MLD_{max} horizon at each of these locations. Although the dominance of this term in the Taylor decomposition is most pronounced at these sites selected to represent regions with exceptionally deep winter mixing, they illustrate the significance of the more general global phenomenon in which the difference between 21st century POC flux changes observed at 100 m versus at the MLD_{max} are predominantly due to the ΔMLD_{max} term, which generally yields an increase in POC flux due to shoaling of the MLD_{max} over the 21st century (Figure 6d).

4. Implications and Conclusions

In this paper, we have analyzed CESM1-BEC output to evaluate the hypothesis that model projected changes to the rate and efficiency of ocean POC flux over the 21st century under RCP8.5 are sensitive to the choice of export depth horizon used for the analysis. This has important implications for the scientific community's ongoing efforts to project how climate change will affect the ocean carbon cycle and feedback on global climate, since prior studies identifying projected decreases in export flux and evaluating underlying mechanistic drivers have focused on evaluating export changes primarily at the

fixed 100 m depth horizon. We show that the MLD_{max} depth horizon, a more appropriate choice for evaluating the effects of POC flux on carbon sequestration into and below the main thermocline, shoals over the 21st century due to warming-driven increases in stratification, decreasing how far particles have to sink in order to be sequestered from contact with the atmosphere on multi-annual time scales (Figure 2).

Despite this shoaling of the MLD_{max} horizon and contrary to our initial hypothesis, the globally-integrated decrease in POC flux and in e-ratio are similar when evaluated at both the MLD_{max} and 100 m depth horizons. Future work will be needed to determine whether this is a consistent result across model formulations or whether this result is specific to the CESM1-BEC simulation assessed here. However, our analysis demonstrates that spatial patterns of change are strongly influenced by the choice of depth horizon (Figures 3-4). Increases in stratification over the 21st century decrease winter mixing in regions with the deepest modern-day MLD_{max}, offsetting ecosystem-driven effects on NPP and e-ratio that drive decreases in POC flux when evaluated at a fixed depth horizon. This ΔMLD_{max} effect tends to increase POC flux by reducing the depth range over which remineralization occurs above the shoaling MLD_{max} horizon that particles must escape in order to be sequestered (Figures 5-7).

The sensitivity of spatial patterns in POC flux change to the choice of export depth horizon has particularly important implications for observational efforts to detect and monitor changes to the biological carbon pump. Our longest-standing time-series sites are located primarily in regions with less extensive winter mixing (e.g. the Hawaii Ocean Time Series and Bermuda Atlantic Time Series), but more recent observational efforts such as Biogeochemical-Argo and the Ocean Observatories Initiative have extended our ability to observe biological carbon fluxes year-round at locations that do experience deep winter mixing (Benway et al., 2019; Roemmich et al., 2019; Trowbridge et al., 2019). Given that projected changes in stratification and MLD_{max} in high latitude regions can have greater influence on changes in export-driven carbon sequestration than ecosystem-driven effects on NPP and e-ratio (Figures 5 and 7), it is critical that these ongoing observational efforts to monitor carbon fluxes consider flux across a range of depths, including MLD_{max}, in order to detect how changes in physics in turn affect the biological pump.

Future work is needed to assess the change in POC flux at MLD_{max} across a range of Earth system model simulations in order to determine the sensitivity of the conclusions presented here to the specific formulations of the marine ecosystem and biogeochemistry dynamics as well as variations in model physics that influence circulation and stratification changes. Previous analysis of the mechanistic drivers of export flux change at 100 m across different Earth system models has shown a wide spread in the magnitude and even directions of change in NPP, particle formation, and remineralization rates (Laufkötter et al., 2016), which may lead to different results across models with different sensitivity to each of these factors contributing to export flux. Further, we recognize that RCP8.5 is a high emissions scenario that is illustrative of the ocean response to a large climate change but not necessarily indicative

of the mostly likely pathway for this century. More moderate RCP scenarios should also be investigated in future work, though it is likely the patterns of physical-biogeochemical response of export at MLD_{max} will be qualitatively similar though quantitatively weaker.

Recent simulations completed for CMIP6 provide an opportunity for the first time to evaluate depth-resolved export flux from a wide range of models (Orr et al., 2016), whereas past model intercomparison projects have only archived POC flux at the 100 m depth horizon, limiting analysis across multiple export depth horizons. Analyses of export flux in CMIP6 output should assess change over time across multiple commonly-used depth horizons, including MLD_{max}, and also take advantage of the full depth resolution to compare full profiles, including remineralization dynamics below the base of the euphotic zone, and consider multiple metrics of transfer and sequestration efficiency in addition to evaluating export rates at individual depth horizons (e.g. Buesseler et al., 2020; Cael & Bisson, 2018; Cavan et al., 2019). Additionally, future analyses of changes to export flux in model simulations should incorporate the contributions zooplankton vertical migration and physical transport of both dissolved and particulate organic carbon to the full biological carbon pump, which have been shown to be important by previous studies that have incorporated these processes into regional and global model studies (Archibald et al., 2019; Resplandy et al., 2019; Roshan & DeVries, 2017).

While we strongly recommend that future analyses of the biological pump in both observational and model analyses evaluate flux at the MLD_{max} depth horizon in order to enable analysis of the influence of this critical process on the global carbon cycle, we also stress that analyses evaluating flux across multiple depth horizons are needed. The MLD_{max} depth horizon provides a realistic metric of multi-annual carbon sequestration that can be used by observationalists, and indeed is being applied in the field (e.g. Bushinsky & Emerson, 2015; Emerson, 2014; Körtzinger et al., 2008; Palevsky, Quay, Lockwood, et al., 2016; Quay et al., 2012; Quay et al., 2020). However, additional information about the time scale of sequestration resulting from circulation and re-entrainment of particles respired throughout the layer below MLD_{max} provides important further context for evaluating the effects of export on longer-term carbon storage (e.g. DeVries et al., 2012; Kwon et al., 2009), and non-linearity in the controls on air-sea CO_2 flux over the seasonal cycle demonstrate the importance of accounting for the timing of fluxes in and out of the mixed layer in order to determine the mechanistic influence of biological carbon export on air-sea CO_2 flux (Fassbender et al., 2018; Palevsky & Quay, 2017). Efforts focused on understanding the ecosystem-based mechanisms of control on the rate and efficiency of the biological pump have also made the case that upper ocean export should be evaluated at the base of the euphotic zone, separating processes in the sunlit surface ocean where both NPP and remineralization occur from the twilight zone below, in which organic carbon is remineralized but no additional production occurs (Buesseler et al., 2020; Buesseler & Boyd, 2009; Lima et al., 2014; Siegel et al., 2016). Observations and data products that incorporate multiple depth horizons, including fully-resolved flux depth profiles where possible, will therefore provide the most robust ability to monitor and mechanistically understand changes to the

ocean's biological carbon pump over time, including interactions between ecosystem-driven processes and physical changes in stratification and circulation that influence sequestration.

5. Acknowledgements

The authors thank Ivan Lima for assistance with identifying and accessing the model output used for this analysis. Model output used here is available at http://www.cesm.ucar.edu/experiments/cesm1.0/ (see section 2.1 for details) and World Ocean Atlas 2013 data used to compare with model output is available at https://www.nodc.noaa.gov/OC5/woa13/. Support for the initial phase of this project was provided by the Woods Hole Oceanographic Institution, with funding to H.I.P. from the Weston Howland Jr. Postdoctoral Scholarship. Model simulations analyzed here were produced as part of the Community Climate/Earth System Model (CCSM/CESM) project supported by the National Science Foundation and the Office of Science (BER) of the United States Department of Energy. The authors thank the scientists, programmers, and software engineers involved in the development and implementation of the CCSM/CESM.

6. References

Archibald, K. M., Siegel, D. A., & Doney, S. C. (2019). Modeling the Impact of Zooplankton Diel Vertical Migration on the Carbon Export Flux of the Biological Pump. *Global Biogeochemical Cycles*, *33*(2), 181–199. https://doi.org/10.1029/2018GB005983

Benway, H. M., Lorenzoni, L., White, A. E., Fiedler, B., Levine, N. M., Nicholson, D. P., et al. (2019). Ocean time series observations of changing marine ecosystems: An era of integration, synthesis, and societal applications. *Frontiers in Marine Science*, *6*(JUL), 1–22. https://doi.org/10.3389/fmars.2019.00393

Bopp, L, Aumont, O., Cadule, P., Alvain, S., & Gehlen, M. (2005). Response of diatoms distribution to global warming and potential implications: A global model study. *Geophys. Res. Lett.*, *32*(19), L19606–L19606. https://doi.org/10.1029/2005GL023653

Bopp, L, Resplandy, L., Orr, J. C., Doney, S. C., Dunne, J. P., Gehlen, M., et al. (2013). Multiple stressors of ocean ecosystems in the 21st century: projections with CMIP5 models. *Biogeosciences*, *10*, 6225–6245. https://doi.org/10.5194/bg-10-6225-2013

Bopp, Laurent, Monfray, P., Aumont, O., Dufresne, J. L., Le Treut, H., Madec, G., et al. (2001). Potential impact of climate change on marine export production. *Global Biogeochemical Cycles*, *15*(1), 81–99. https://doi.org/10.1029/1999GB001256

Boyd, P. W., Claustre, H., Levy, M., Siegel, D. A., & Weber, T. (2019). Multi-faceted particle pumps drive carbon sequestration in the ocean. *Nature*, *568*(7752), 327–335. https://doi.org/10.1038/s41586-019-1098-2

Buesseler, K. O., & Boyd, P. W. (2009). Shedding light on processes that control particle export and flux attenuation in the twilight zone of the open ocean. *Limnology and Oceanography*, *54*(4), 1210–1232. https://doi.org/10.4319/lo.2009.54.4.1210

Buesseler, K. O., Boyd, P. W., Black, E. E., & Siegel, D. A. (2020). Metrics that matter for assessing the ocean biological carbon pump, *117*(18), 9679–9687. https://doi.org/10.1073/pnas.1918114117

Bushinsky, S. M., & Emerson, S. (2015). Marine biological production from in situ oxygen measurements on a profiling float in the subarctic Pacific Ocean. *Global Biogeochemical Cycles*, *29*(12), 2050–2060. https://doi.org/10.1002/2015GB005251

Cabré, A., Marinov, I., & Leung, S. (2015). Consistent global responses of marine ecosystems to future

climate change across the IPCC AR5 earth system models. *Climate Dynamics*, *45*(5–6), 1253–1280. https://doi.org/10.1007/s00382-014-2374-3

Cael, B. B., & Bisson, K. (2018). Particle flux parameterizations: Quantitative and mechanistic similarities and differences. *Frontiers in Marine Science*, *5*(OCT), 1–5. https://doi.org/10.3389/fmars.2018.00395

Capotondi, A., Alexander, M. A., Bond, N. A., Curchitser, E. N., & Scott, J. D. (2012). Enhanced upper ocean stratification with climate change in the CMIP3 models. *Journal of Geophysical Research: Oceans*, *117*(4), 1–23. https://doi.org/10.1029/2011JC007409

Cavan, E. L., Laurenceau-Cornec, E. C., Bressac, M., & Boyd, P. W. (2019). Exploring the ecology of the mesopelagic biological pump. *Progress in Oceanography*, *176*(June), 102125. https://doi.org/10.1016/j.pocean.2019.102125

Cheng, W., Chiang, J. C. H., & Zhang, D. (2013). Atlantic meridional overturning circulation (AMOC) in CMIP5 Models: RCP and historical simulations. *Journal of Climate*, *26*(18), 7187–7197. https://doi.org/10.1175/JCLI-D-12-00496.1

DeVries, T., Primeau, F., & Deutsch, C. (2012). The sequestration efficiency of the biological pump. *Geophysical Research Letters*, *39*, L13601–L13601. https://doi.org/10.1029/2012GL051963

Doney, S. C., Lima, I., Moore, J. K., Lindsay, K., Behrenfeld, M. J., Westberry, T. K., et al. (2009). Skill metrics for confronting global upper ocean ecosystem-biogeochemistry models against field and remote sensing data. *Journal of Marine Systems*, *76*(1–2), 95–112. https://doi.org/10.1016/j.jmarsys.2008.05.015

Dunne, J. P., Armstrong, R. A., Gnanadesikan, A., & Sarmiento, J. L. (2005). Empirical and mechanistic models for the particle export ratio. *Global Biogeochem. Cycles*, *19*. https://doi.org/10.1029/2004GB002390

Dunne, J. P., Sarmiento, J. L., & Gnanadesikan, A. (2007). A synthesis of global particle export from the surface ocean and cycling through the ocean interior and on the seafloor. *Global Biogeochem. Cycles*, *21*(4). https://doi.org/10.1029/2006GB002907

Emerson, S. (2014). Annual Net Community Production and the Biological Carbon Flux in the Ocean. *Global Biogeochemical Cycles*, *28*. https://doi.org/10.1002/2013GB004680

Fassbender, A. J., Rodgers, K. B., Palevsky, H. I., & Sabine, C. L. (2018). Seasonal Asymmetry in the Evolution of Surface Ocean pCO2 and pH Thermodynamic Drivers and the Influence on Sea-Air CO2 Flux. *Global Biogeochemical Cycles*, *32*(10), 1476–1497. https://doi.org/10.1029/2017GB005855

Friedlingstein, P., Jones, M. W., O'Sullivan, M., Andrew, R. M., Hauck, J., Peters, G. P., et al. (2019). Global carbon budget 2019. *Earth System Science Data*, *11*(4), 1783–1838. https://doi.org/10.3929/ethz-a-010782581

Fu, W., Randerson, J. T., & Keith Moore, J. (2016). Climate change impacts on net primary production (NPP) and export production (EP) regulated by increasing stratification and phytoplankton community structure in the CMIP5 models. *Biogeosciences*, *13*(18), 5151–5170. https://doi.org/10.5194/bg-13-5151-2016

Fung, I. Y., Doney, S. C., Lindsay, K., & John, J. (2005). Evolution of carbon sinks in a changing climate, *102*(32), 11201–11206.

Gent, P. R., Danabasoglu, G., Donner, L. J., Holland, M. M., Hunke, E. C., Jayne, S. R., et al. (2011). The community climate system model version 4. *Journal of Climate*, *24*(19), 4973–4991. https://doi.org/10.1175/2011JCLI4083.1

Giering, S. L. C., & Humphreys, M. P. (2018). Biological pump. *Encyclopedia of Earth Sciences Series*, 111–116. https://doi.org/10.1007/978-3-319-39312-4_154

Henson, S. a., Sanders, R., & Madsen, E. (2012). Global patterns in efficiency of particulate organic carbon export and transfer to the deep ocean. *Global Biogeochemical Cycles*, *26*(1), 1–14. https://doi.org/10.1029/2011GB004099

Henson, S. A., Sanders, R., Madsen, E., Morris, P. J., Le Moigne, F., & Quartly, G. D. (2011). A reduced estimate of the strength of the ocean's biological carbon pump. *Geophysical Research Letters*,

38(4), 10–14. https://doi.org/10.1029/2011GL046735
Körtzinger, A., Send, U., Lampitt, R. S., Hartman, S., Wallace, D. W. R., Karstensen, J., et al. (2008). The seasonal pCO_2 cycle at 49°N/16.5°W in the northeastern Atlantic Ocean and what it tells us about biological productivity. *Journal of Geophysical Research*, *113*, C04020–C04020. https://doi.org/10.1029/2007JC004347
Kwon, E. Y., Primeau, F., & Sarmiento, J. L. (2009). The impact of remineralization depth on the air–sea carbon balance. *Nature Geoscience*, *2*(9), 630–635. https://doi.org/10.1038/ngeo612
Lam, P. J., Doney, S. C., & Bishop, J. K. B. (2011). The dynamic ocean biological pump: Insights from a global compilation of particulate organic carbon, CaCO 3, and opal concentration profiles from the mesopelagic. *Global Biogeochemical Cycles*, *25*, GB3009–GB3009. https://doi.org/10.1029/2010GB003868
Laufkötter, C., Vogt, M., Gruber, N., Aita-Noguchi, M., Aumont, O., Bopp, L., et al. (2015). Drivers and uncertainties of future global marine primary production in marine ecosystem models. *Biogeosciences*, *12*(23), 6955–6984. https://doi.org/10.5194/bg-12-6955-2015
Laufkötter, Charlotte, Vogt, M., Gruber, N., Aumont, O., Bopp, L., Doney, S. C., et al. (2016). Projected decreases in future marine export production: The role of the carbon flux through the upper ocean ecosystem. *Biogeosciences*, *13*(13), 4023–4047. https://doi.org/10.5194/bg-13-4023-2016
Laws, E A, Falkowski, P. G., Smith, W. O. J., Ducklow, H., & McCarthy, J. J. (2000). Temperature effects on export production in the open ocean. *Global Biogeochem. Cycles*, *14*(4), 1231–1246.
Laws, Edward A, D'Sa, E., & Naik, P. (2011). Simple equations to estimate ratios of new or export production to total production from satellite-derived estimates of sea surface temperature and primary production. *Limnology and Oceanography: Methods*, *9*, 593–601. https://doi.org/10.4319/lom.2011.9.593
Leung, S., Cabre, A., & Marinov, I. (2015). A latitudinally banded phytoplankton response to 21st century climate change in the Southern Ocean across the CMIP5 model suite. *Biogeosciences*, *12*(19), 5715–5734. https://doi.org/10.5194/bg-12-5715-2015
Lima, I. D., Lam, P. J., & Doney, S. C. (2014). Dynamics of particulate organic carbon flux in a global ocean model. *Biogeosciences*, *11*, 1177–1198. https://doi.org/10.5194/bg-11-1177-2014
Lindsay, K., Bonan, G. B., Doney, S. C., Hoffman, F. M., Lawrence, D. M., Long, M. C., et al. (2014). Preindustrial-control and twentieth-century carbon cycle experiments with the Earth system model CESM1(BGC). *Journal of Climate*, *27*(24), 8981–9005. https://doi.org/10.1175/JCLI-D-12-00565.1
Marinov, I., Doney, S. C., Lima, I. D., Lindsay, K., Moore, J. K., & Mahowald, N. (2013). North-South asymmetry in the modeled phytoplankton community response to climate change over the 21st century, *27*(February), 1274–1290. https://doi.org/10.1002/2013GB004599
Marsay, C. M., Sanders, R. J., Henson, S. A., Pabortsava, K., Achterberg, E. P., & Lampitt, R. S. (2015). Attenuation of sinking particulate organic carbon flux through the mesopelagic ocean. *Proceedings of the National Academy of Sciences of the United States of America*, *112*(4), 1089–1094. https://doi.org/10.1073/pnas.1415311112
Le Moigne, F. A. C. (2019). Pathways of Organic Carbon Downward Transport by the Oceanic Biological Carbon Pump. *Frontiers in Marine Science*, *6*(October), 1–8. https://doi.org/10.3389/fmars.2019.00634
Moore, J. K., Doney, S. C., & Lindsay, K. (2004). Upper ocean ecosystem dynamics and iron cycling in a global three-dimensional model. *Global Biogeochemical Cycles*, *18*(4), 1–21. https://doi.org/10.1029/2004GB002220
Moore, J. K., Lindsay, K., Doney, S. C., Long, M. C., & Misumi, K. (2013). Marine ecosystem dynamics and biogeochemical cycling in the community earth system model [CESM1(BGC)]: Comparison of the 1990s with the 2090s under the RCP4.5 and RCP8.5 scenarios. *Journal of Climate*, *26*(23), 9291–9312. https://doi.org/10.1175/JCLI-D-12-00566.1
Orr, J. C., Najjar, R. G., Aumount, O., Bopp, L., Bullister, J. L., Danabasoglu, G., et al. (2016). Biogeochemical protocols and diagnostics for the CMIP6 Ocean Model Intercomparison Project (OMIP). *Geoscientific Model Development Discussions*, *0*(July), 1–45. https://doi.org/10.5194/gmd-

675 2016-155
676 Oschlies, A., Schulz, K. G., Riebesell, U., & Schmittner, A. (2008). Simulated 21st century's increase in
677 oceanic suboxia by CO 2-enhanced biotic carbon export. *Global Biogeochemical Cycles*, *22*(4), 1–
678 10. https://doi.org/10.1029/2007GB003147
679 Palevsky, H I, Quay, P. D., & Nicholson, D. P. (2016). Discrepant estimates of primary and export
680 production from satellite algorithms, a biogeochemical model, and geochemical tracer
681 measurements in the North Pacific Ocean. *Geophysical Research Letters*, *43*(16).
682 https://doi.org/10.1002/2016GL070226
683 Palevsky, Hilary I., & Doney, S. C. (2018). How Choice of Depth Horizon Influences the Estimated
684 Spatial Patterns and Global Magnitude of Ocean Carbon Export Flux. *Geophysical Research*
685 *Letters*, *45*(9), 4171–4179. https://doi.org/10.1029/2017GL076498
686 Palevsky, Hilary I., & Quay, P. D. (2017). Influence of biological carbon export on ocean carbon uptake
687 over the annual cycle across the North Pacific Ocean. *Global Biogeochemical Cycles*, *31*(1), 81–95.
688 https://doi.org/10.1002/2016GB005527
689 Palevsky, Hilary I, Quay, P., Lockwood, D. E., & Nicholson, D. P. (2016). The annual cycle of gross
690 primary production, net community production, and export efficiency across the North Pacific
691 Ocean. *Global Biogeochemical Cycles*, *30*(2). https://doi.org/10.1002/2015GB005318
692 Quay, P, Stutsman, J., & Steinhoff, T. (2012). Primary production and carbon export rates across the
693 subpolar N. Atlantic Ocean basin based on triple oxygen isotope and dissolved O2 and Ar gas
694 measurements. *Global Biogeochemical Cycles*, *26*, GB2003–GB2003.
695 https://doi.org/10.1029/2010GB004003
696 Quay, Paul, Emerson, S., & Palevsky, H. I. (2020). Regional pattern of the ocean's biological pump based
697 on geochemical observations. *Geophys. Res. Lett.*
698 https://doi.org/https://doi.org/10.1029/2020GL088098
699 Resplandy, L., Lévy, M., & McGillicuddy, D. J. (2019). Effects of Eddy-Driven Subduction on Ocean
700 Biological Carbon Pump. *Global Biogeochemical Cycles*, *33*(8), 1071–1084.
701 https://doi.org/10.1029/2018GB006125
702 Roemmich, D., Alford, M. H., Claustre, H., Johnson, K. S., King, B., Moum, J., et al. (2019). On the
703 future of Argo: A global, full-depth, multi-disciplinary array. *Frontiers in Marine Science*, *6*(JUL),
704 1–28. https://doi.org/10.3389/fmars.2019.00439
705 Roshan, S., & DeVries, T. (2017). Efficient dissolved organic carbon production and export in the
706 oligotrophic ocean. *Nature Communications*, *8*(1), 2036. https://doi.org/10.1038/s41467-017-02227-
707 3
708 Sallée, J. B., Shuckburgh, E., Bruneau, N., Meijers, A. J. S., Bracegirdle, T. J., & Wang, Z. (2013).
709 Assessment of Southern Ocean mixed-layer depths in CMIP5 models: Historical bias and forcing
710 response. *Journal of Geophysical Research: Oceans*, *118*(4), 1845–1862.
711 https://doi.org/10.1002/jgrc.20157
712 Schmittner, A., Oschlies, A., Matthews, H. D., & Galbraith, E. D. (2008). Future changes in climate,
713 ocean circulation, ecosystems, and biogeochemical cycling simulated for a business-as-usual CO2
714 emission scenario until year 4000 AD. *Global Biogeochem. Cycles*, *22*, GB1013–GB1013.
715 https://doi.org/10.1029/2007GB002953
716 Siegel, D A, Buesseler, K. O., Doney, S. C., Sailley, S. F., Behrenfeld, M. J., & Boyd, P. W. (2014).
717 Global assessment of ocean carbon export by combining satellite observations and food-web
718 models. *Global Biogeochemical Cycles*, *28*, 181–196. https://doi.org/10.1002/2013GB004743
719 Siegel, David A, Buesseler, K. O., Behrenfeld, M. J., Benitez-Nelson, C. R., Boss, E., Brzezinski, M. A.,
720 et al. (2016). Prediction of the Export and Fate of Global Ocean Net Primary Production: The
721 EXPORTS Science Plan. *Frontiers in Marine Science*, *3*(22).
722 https://doi.org/10.3389/fmars.2016.00022
723 Steinacher, M., Joos, F., Frolicher, T. L., Bopp, L., Cadule, P., Cocco, V., et al. (2010). Projected 21st
724 century decrease in marine productivity: a multi-model analysis. *Biogeosciences*, *7*, 979–1005.
725 Taucher, J., & Oschlies, A. (2011). Can we predict the direction of marine primary production change

under global warming? *Geophys. Res. Lett.*, *38*(L02603). https://doi.org/10.1029/2010GL045934
Trowbridge, J., Weller, R., Kelley, D., Dever, E., Plueddemann, A., Barth, J. A., & Kawka, O. (2019). The ocean observatories initiative. *Frontiers in Marine Science*, *6*(MAR), 1–23. https://doi.org/10.3389/fmars.2019.00074
Volk, T., & Hoffert, M. I. (1985). Ocean Carbon Pumps: Analysis of relative strengths and efficiencies in ocean-driven atmospheric CO_2 changes. In E. T. Sundquist & W. S. Broecker (Eds.), *The Carbon Cycle and Atmospheric CO_2 Natural Variations Archean to Present* (Vol. 32, pp. 99–110). American Geophysical Union, Wahington, DC.